International Journal of Heat and Mass Transfer 188 (2022) 122598

Contents lists available at ScienceDirect

International Journal of Heat and Mass Transfer

journal homepage: www.elsevier.com/locate/hmt

Heat and mass transfer in laminar falling film absorption: A compact analytical model

Mahyar Ashouri, Majid Bahrami*

Laboratory for Alternative Energy Conversion (LAEC), School of Mechatronic Systems Engineering, Simon Fraser University, Surrey, British Columbia V3T 0A3, Canada

ARTICLE INFO

Article history:
Received 27 September 2021
Revised 29 December 2021
Accepted 19 January 2022
Available online 5 February 2022

Keywords:
Absorption system
Analytical solution
Falling film
Heat and mass transfer
Non-volatile absorbents
Laplace transform

ABSTRACT

Absorption process plays a significant role in numerous industrial applications. Several analytical solutions have been proposed for the absorption process to calculate heat and mass transfer rates in falling film absorbers. However, the existing analytical solutions are either complex or do not consider the initial and boundary conditions at the entrance region and/or are not accurate enough. In this study, a new analytical solution for non-volatile absorbents is presented using the Laplace transform method by proposing a new velocity profile for falling films. Moreover, for the first time, compact relationships are proposed to calculate the heat and mass transfer rates in the falling film absorption process for four common absorber geometries, including: (i) inclined plates; (ii) tube bundles absorbers; (iii) vertical tubes; and (iv) coil type absorbers. The proposed compact relationships are validated with experimental data collected by others with reasonable accuracy. Furthermore, a parametric study is conducted to investigate the impact of input parameters on the absorption rate of falling film on an inclined plate. It is observed that the concentration of inlet solution is the most effective parameter and the solution mass flow rate has the least impact.

1. Introduction

Climate change has become one of the most important concerns of the world in recent years. Fossil fuels are consumed as the main energy resource in residential buildings and industrial processes [1,2]. Approximately 40% of the total energy consumption in developed countries is associated with buildings of which approximately 70% is used for domestic hot water and space heating and cooling [3,4]. Vapor compression refrigeration systems, the most commonly used heat pumping and air conditioning system, consume nearly 15% of the global electricity, up to 76% of which is generated preponderantly from fossil fuels [5]. It is crucial to develop alternative sustainable heating/cooling solutions to reduce fossil fuel consumption and their associated impact on climate change. A heat-driven absorption process can be a promising alternative option for heating and cooling applications, including heat pumps, air conditioning systems, and heat transformers to upgrade low-grade heat. It also can be implemented in other applications, such as CO_2 capture, thermal storage, and dehumidification systems [6–9]. Absorption systems are cost-effective and may be operated by waste or low grade heat [10]. However, there are still challenges with the existing absorption systems, including: (i) corrosion [11]; (ii) crystallization [12]; and (iii) low performance (for absorption chillers and heat pumps) leading to bulky and heavy units. These challenges may be remedied, e.g., some methods have been proposed to prevent corrosion by using a coating [13] or to prevent crystallization by implementing proper control strategies [14].

The absorber is the key part of the absorption cycle/process. Perhaps, the main challenge to making absorption heat transformers (AHTs) economically competitive with vapor compression systems is to significantly advance the performance of the absorbers. Heat and mass transfer (HMT) simultaneously occur in absorbers; thus, developing an in-depth understanding of pertinent HMT phenomena is key for the development of efficient and durable AHTs.

There are several numerical studies available in the literature on analyzing falling films in absorbers, which is one the most common designs in currently available absorption systems [15]. Numerical analysis [16] and simulations can be used for the absorber design and provide detailed results when properly set and used. However, implementing numerical methods requires high computational time and their results are restricted to a specific geometry or design (with the selected operating conditions) which could reduce their usability. Furthermore, accurate and compact relationships are needed for real-time control to enable system operation

Abbreviations: CBL, concentration boundary layer; HMT, heat and mass transfer; LEA, le.Λ^{-1}; LTM, Laplace transform method; TBL, thermal boundary layer.

* Corresponding author.
E-mail address: mbahrami@sfu.ca (M. Bahrami).

https://doi.org/10.1016/j.ijheatmasstransfer.2022.122598
0017-9310/

Nomenclature

c	concentration of adsorbate, $kg.kg^{-1}$
c_s	isobaric specific heat, $J•kg^{-1}K^{-1}$
D_s	mass diffusivity, $m^2•s^{-1}$
g	gravity, $m•s^{-2}$
Le	lewis number, $[Le=\alpha.D^{-1}]$
L	length, m
L_c	characteristic length, m
N_{tube}	number of tubes
$\dot{m}$	absorption rate, $kg•m^{-2}s^{-1}$
$\dot{q}$	heat flux, $W•m^{-2}$
T	temperature, K
u	streamwise velocity, $m•s^{-1}$
v	normal velocity, $m•s^{-1}$
x	local tangential position, m
y	local normal position, m

Greek symbols

α	thermal diffusivity, $m^2•s^{-1}$
φ	angle
γ	dimensionless mass fraction distribution
η	dimensionless normal position
Λ	normalized heat of absorption
θ	dimensionless temperature distribution
δ	film thickness, m
ρ	density, $kg•m^{-3}$
ν	kinematic viscosity, $m^2•s^{-1}$

Subscripts

eq	equilibrium
inf	interface
l	local
o	entrance region
s	solution
t	total
w	wall

and performance optimization under actual operating conditions as they vary over time.

On the other hand, analytical solutions [17] are few and far between in the literature. Analytical methods are preferred – when possible to find – since they provide a generalized solution that makes design optimization, real-time control, and parametric studies possible in a timely fashion. Three different analytical methods were proposed for solving the coupled HMT in laminar falling film absorption over vertical plates and horizontal tubes absorption process in the literature, summarized in Table 1. These models are based on: (i) the similarity solution [18]; (ii) the Fourier method [19]; and (iii) the Laplace transform method (LTM) [20].

Nakoryakov and Grigor'eva [21] proposed a closed-form solution for the coupled HMT in falling film absorption over horizontal tubes. Considering a linear equilibrium equation at the interface between the solution film and gaseous phase, see Eq. (1), and an impermeable isothermal wall, they utilized a similarity solution method to evaluate the temperature and concentration profiles in falling film. Also, they reported that the temperature profile was linear.

$$c = aT + b \tag{1}$$

where, c and T are concentration and temperature, and a and b represent the corresponding constants, respectively. In another study, Nakoryakov et al. [18] analyzed HMT at the entrance region of the falling film over a vertical plate, and reported that the entrance region was controlled by Froude, Peclet, and Lewis numbers, as well as phase transition criterion for absorption. Assuming a hydrodynamically fully-developed flow, remarkably high Schmidt number, and linear equilibrium assumption at the solution-gas interface, Giannetti et al. [26] investigated HMT in a falling film over a horizontal tube using both similarity and numerical methods. Comparing the numerical results and analytical solution, it was shown that their analytical expression can approximately estimate the temperature and concentration profiles, yet the analytical solution error was higher, especially at the entrance region of the falling film.

Grossman [28] analytically solved coupled HMT for a laminar falling film over a vertical plate under both isothermal and adiabatic boundary conditions using the Fourier method. Assuming a fully-developed hydrodynamic boundary layer, he obtained two series solutions to predict the temperature and concentration in the film. The solution was not accurate for the small values of the normalized coordinate in the flow direction, i.e., the developing flow at the entrance region of the falling film. To surmount this issue, he developed another analytical solution using a similarity solution method to estimate the temperature and concentration distributions within the film for the region adjacent to the entrance region. Using a procedure analogous to Grossman [28], Giannetti et al. [10] proposed an analytical solution for falling film absorption over a horizontal tube and examined the impact of the film thickness variation and partial wetting ratio on the mass transfer rate as well.

Other studies, see e.g., [20,33], have been conducted to investigate the coupled HMT in falling film using the LTM. Assuming a high Schmidt number, a closed-form solution for the Sherwood number was proposed in falling film over a vertical plate by Conlisk [33]. Also, Conlisk and Mao [34] extended this model for transient heat transfer using the Fourier transform method. Meyer and Ziegler [30] used LTM to solve the coupled HMT in falling film over a horizontal tube. Assuming a uniform velocity profile and a constant film thickness, they introduced an analytical solution that could be applied to various conditions considering linear equilibrium assumption or other phase equilibrium assumptions. In another study, Meyer [31] scrutinized the influence of a diabatic wall on HMT in falling film over a vertical plate to find a more realistic model. Mortazavi and Moghaddam [32] analyzed the impact of a linear velocity profile on the film temperature and concentration profiles using the LTM. It was concluded that a uniform velocity profile assumption: (i) overestimates the solvent concentration; and (ii) underestimates the solvent temperature and the amount of absorbed gas at the interface between the solution film and gaseous phase.

Based on the above literature survey, one may conclude that: (i) the similarity solution method does not result in accurate results, especially at the entrance region because there is no similarity between the profiles in this region, to be discussed later in more detail; (ii) although, analytical solutions obtained by the Fourier method provide reasonable accuracy, the eigenvalues should be numerically calculated for each operating condition, which makes it difficult to use under operating conditions in real systems; and (iii) the LTM method can result in a solution with reasonable accuracy provided that a suitable velocity profile is used.

In this study, a new analytical solution for the coupled HMT in falling film absorption based on the LTM is developed. In previous works, either uniform or linear velocity profiles have been assumed to solve the problem via the LTM. Here, a new velocity profile is proposed that leads to more accurate results. The proposed solution provides temperature and concentration distributions for the entire falling film domain. In addition, for the first time, compact relationships are proposed for calculating local and total HMT rates for several absorber geometries, namely, the inclined plate, vertical tube, tube bundles absorber, and the coil type absorber under various operating conditions.

Table 1
Existing analytical solutions for coupled HMT in laminar falling film absorption over vertical plates and horizontal tubes.

Solution Method	Study	Configuration	Main limitations/improvements	Advantages/disadvantages
Similarity solution	Nakoryakov and Grigor'eva [21]	Vertical plate	- Uniform velocity profile - Linear temperature profile	+ Compact equation for temperature and concentration profiles. + Compact equation for Sherwood and Nusselt numbers. - Relatively high error due to assuming uniform velocity profile.
	Nakoryakov and Grigor'eva [22]	Vertical plate	- Uniform velocity profile - Neglecting wall temperature	- The temperature profiles are not similar in a falling film so using this method results in finding inaccurate temperature profiles especially at the entrance region. This assumption can lead to notable solution error in HMT rates, in particular, at the entrance region.
	Nakoryakov and Grigor'eva [23]	Vertical plate	- Uniform velocity profile - Linear temperature profile	
	Grossman [24]	Vertical plate	- Uniform velocity profile - Only applicable for the entrance region of falling film	
	Brauner et al. [25]	Vertical plate	- Uniform velocity profile	
	Nakoryakov et al. [18]	Vertical plate	- Uniform velocity profile - Only applicable for the entrance region of a falling film + Variable film thickness	
	Giannetti [26]	Horizontal tube	- Uniform velocity profile	
Fourier method/ Expansion series	Grigor'eva and Nakoryakov [27]	Vertical plate	- Uniform velocity profile	+ Closed-form solution for temperature and concentration profiles. + Closed-form solution for Sherwood and Nusselt numbers.
	Grossman [28]	Vertical plate	+ Parabolic velocity profile	+ Good accuracy except for the entrance region of falling film - Inconsistency of the initial and boundary conditions at the entrance region of falling film results in low accuracy at this region. - Complexity of implementing, such as numerically finding eigenvalues for various operating conditions.
	Nakoryakov et al. [29]	Vertical plate	- Uniform velocity profile	
	Giannetti et al. [10]	Horizontal tube	+ Parabolic velocity profile + Partial wetting	
Laplace transform method	Meyer and Ziegler [30]	Vertical plate	- Uniform velocity profile	+ Closed-form solution for temperature and concentration profiles. + Closed-form solution for Sherwood and Nusselt numbers.
	Meyer [31]	Vertical plate	- Uniform velocity profile + Adding the effect of the Biot number	- Low accuracy because of using uniform profiles.
	Mortazavi and Moghaddam [32]	Vertical plate	+ Linear velocity profile	+ Closed-form solution for temperature and concentration profiles. - Low accuracy because of using linear profiles.
	This study	Inclined plate	+ Parabolic velocity profile + Not restricted to a specific geometry	+ Closed-form solution for temperature and concentration profiles. + Compact equations for HMT rates in falling film absorption over vertical/inclined plate, vertical tube, horizontal tube, and coil type absorber. + High accuracy because of using parabolic velocity profile.

2. Problem description and assumptions

Coupled HMT in laminar falling film absorption over an inclined plate is investigated, as schematically shown in Fig. 1. Later, it is shown how this solution can be extended and applied to vertical and horizontal tubes.

The solution is introduced at the top of the plate with a uniform inlet temperature "T_o" and concentration "c_o" and forms a continuous film. Although, LiBr-water, a commonly used fluid for refrigeration applications, is considered as the working fluid, the present analytical model can be generalized for other types of non-volatile solutions. The film is exposed to water vapor (gaseous phase). The absorption process is exothermic, so heat is generated at the interface between the solution film and gaseous phase. Thus, as shown in Fig. 1, two thermal boundary layers (TBL) are formed: (i) a TBL adjacent to the wall, as a result of the temperature difference between the wall and film temperatures; and (ii) another TBL in the vicinity of the interface, as a consequence of the temperature difference between the working fluid and the interface temperatures. In addition, a Concentration Boundary Layer (CBL) is formed at the vapor-solution interface due to vapor absorption.

The following summarizes the present model assumptions [30]:

- The solution film is in laminar regime and the flow is hydrodynamically fully developed (LiBr-water→Pr∼20–30 [26], LiCl-water→Pr∼35 [35]).
- Thermo-physical properties are constant throughout the entire domain.
- The absorbent is non-volatile.
- Heat transfer from the film to the gas phase is neglected.
- The mass flow rate variation as a result of the absorbed gas is negligible.
- The drag force at the interface is negligible.
- There is no disturbance or wave at the interface.

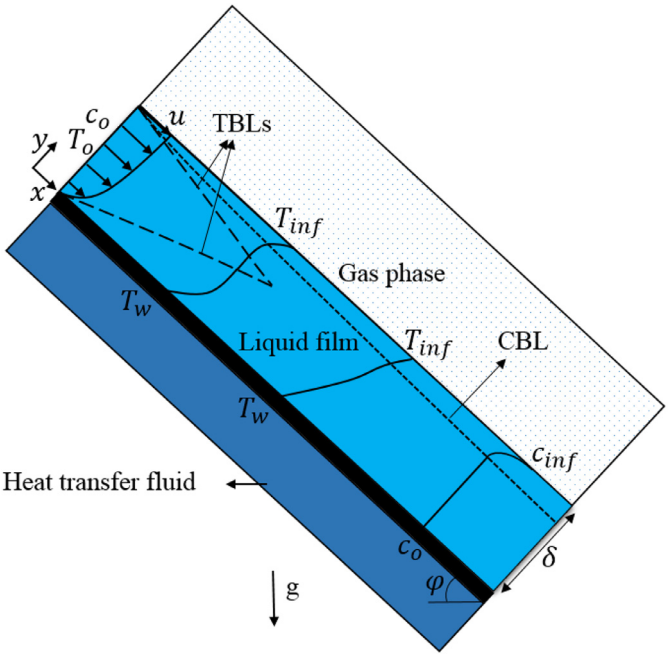

Fig. 1. The schematic diagram of falling film absorption over an inclined plate.

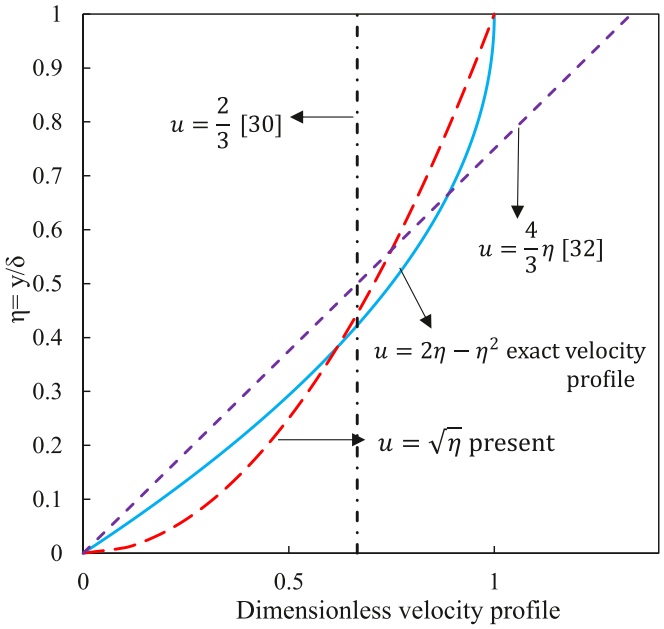

Fig. 2. A comparison between different velocity profiles versus η.

- Temperature and concentration distributions are uniform at the entrance region.
- The wall is considered isothermal; and.
- Linear equilibrium assumption exists at the solution-vapor interface, and equilibrium can be approximated with a linear equation [26,28,31].

3. Model development

3.1. Governing equations and boundary conditions

Continuity and momentum equations are as follows [36]:

$$\frac{\partial u}{\partial x} + \frac{\partial v}{\partial y} = 0 \tag{2}$$

$$u\frac{\partial u}{\partial x} + v\frac{\partial u}{\partial y} = gsin(\varphi) + \nu\frac{\partial^2 u}{\partial y^2} \tag{3}$$

where, u and v are streamwise velocity and velocity perpendicular to the plate; g, φ, and ν are gravitational acceleration, tilt angle of the plate, and kinematic viscosity, respectively.

For the hydrodynamically fully developed region, velocity in the direction perpendicular to the plate is zero, i.e., $v = 0$. The thickness of the hydrodynamic boundary layer and the velocity profile can be found as follows, respectively, [10]:

$$\delta = \left(\frac{3\Gamma\nu}{g\rho sin(\varphi)}\right)^{1/3} [m] \tag{4}$$

$$u = \frac{3}{2}\bar{u}\left(2\eta - \eta^2\right)\left[\frac{m}{s}\right] \tag{5}$$

$$\bar{u} = \frac{\Gamma}{\rho\delta} \tag{6}$$

$$\eta = \frac{y}{\delta} \tag{7}$$

where, δ, η, and $\bar{u}$ are boundary layer thickness, non-dimensional "y", and average velocity, respectively. Also, ρ and Γ denote the solution density and solution mass flow rate per unit length, respectively. Given the convective transport in the flow (x-direction) and diffusivity transport in the y-direction, the following governing equations for energy and solution mass balance (concentration) can be derived:

$$u\frac{\partial T}{\partial x} = \alpha\frac{\partial^2 T}{\partial y^2} \tag{8}$$

$$u\frac{\partial c}{\partial x} = D_s\frac{\partial^2 c}{\partial y^2} \tag{9}$$

where, T, α, c, and D_s are temperature, thermal diffusivity, absorbate concentration, and mass diffusivity, respectively. Considering the LTM, it is not possible to solve this problem using a fully developed velocity profile, Eq. (5). After notable investigations and curve fitting by considering a functional form for the velocity profile to obtain an analytical solution using the LTM, the following velocity profile is obtained and proposed here:

$$u = \frac{3}{2}\bar{u}\sqrt{\eta}\left[\frac{m}{s}\right] \tag{10}$$

Fig. 2 shows a comparison between uniform [30], linear [32], and the proposed velocity profiles. The following equation is used as a criterion to assess the relative difference of the mentioned velocity profiles compared to the velocity profile obtained by exact solution (Eq. (5))

$$mean\ difference\ (\%) = \frac{\sum_{i=0}^{N}\left|u_{exact}\left(\eta = \frac{i}{N}\right) - u_{estimated}\left(\eta = \frac{i}{N}\right)\right|}{\sum_{i=0}^{N}\left|u_{exact}\left(\eta = \frac{i}{N}\right)\right|} \times 100 \tag{11}$$

The mean relative differences between the exact solution, Eq. (5), and uniform [30], linear [32], and the proposed velocity profiles are 38.95%, 14.94%, and 8.92%, respectively, which indicates that the proposed velocity profile is in better agreement with the exact velocity profile.

Using the equilibrium temperature and concentration, Eqs. (8) and (9) can be non- dimensionalized. The equilibrium temperature "T_{eq}" is the temperature corresponding to the concentration at the entrance "c_o", and, similarly, the equilibrium

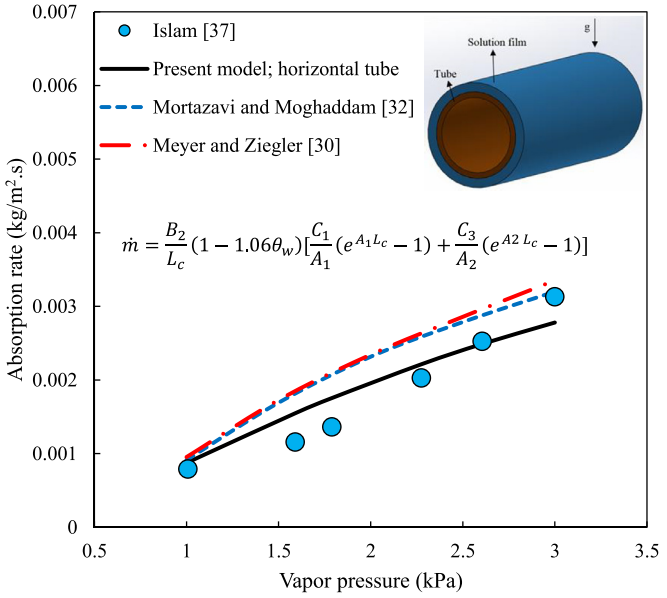

Fig. 3. Absorption rate variation versus vapor pressure calculated using the present model Eq. (30), the analytical model of Meyer and Ziegler [30] (Eq. (51) in Ref. [30]), and the analytical model of Mortazavi and Moghaddam [32] (Eq. (42) in Ref. [32]) compared against the experimental data from Islam [37].

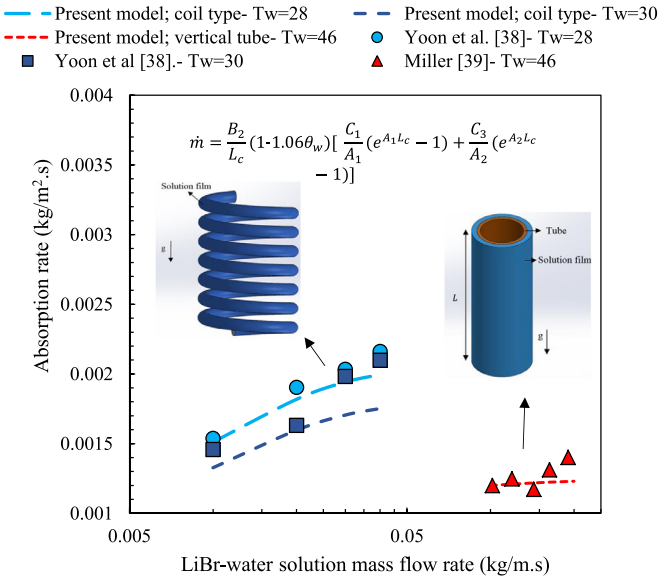

Fig. 4. Absorption rate variation versus LiBr-water solution mass flow rate calculated using the present model (Eq. (30)), compared against experimental data from Yoon et al. [38], Miller and Perez-Blanco [39].

concentration "c_{eq}" is the concentration corresponding to the temperature at the entrance "T_o". Equilibrium temperature and concentration can be calculated via a phase equilibrium equation; see Appendix. A. Thanks to the functional form for the proposed approximate velocity profile (see Eq. (10)), non-dimensional energy and mass balance equations can be derived as follows:

$$\sqrt{\eta}\frac{\partial\theta}{\partial\xi} = \frac{\partial^2\theta}{\partial\eta^2} \tag{12}$$

$$Le\sqrt{\eta}\frac{\partial\gamma}{\partial\xi} = \frac{\partial^2\gamma}{\partial\eta^2} \tag{13}$$

$$\theta(\xi,\eta) = \frac{T(\xi,\eta)-T_o}{T_{eq}(c_o,p)-T_o} \tag{14}$$

$$\gamma(\xi,\eta) = \frac{c(\xi,\eta)-c_o}{c_{eq}(T_o,p)-c_o} \tag{15}$$

$$\xi = \frac{x}{\delta^2}\frac{\alpha}{\frac{3}{2}\bar{u}},\quad \eta = \frac{y}{\delta} \tag{16}$$

where, θ, γ, and ξ represent non-dimensional temperature, non-dimensional concentration, non-dimensional "x", respectively. Initial and boundary conditions considering isothermal and impermeable wall are [30]:

$$\theta(0,\eta) = \frac{T_o-T_o}{T_{eq}(c_o,p)-T_o} = 0 \tag{17}$$

$$\gamma(0,\eta) = \frac{c_o-c_0}{c_{eq}(T_o,p)-c_o} = 0 \tag{18}$$

$$\theta(\xi,0) = \frac{T_w-T_o}{T_{eq}(c_o,p)-T_o} = \theta_w \tag{19}$$

$$\frac{\partial\gamma}{\partial\eta}|_{\eta=0} = 0 \tag{20}$$

$$\theta(\xi,1)+\gamma(\xi,1) = 1 \tag{21}$$

$$\frac{\partial\theta}{\partial\eta}|_{inf} = \frac{\Lambda}{Le}\frac{\partial\ \gamma}{\partial\eta}|_{inf} \tag{22}$$

$$\Lambda = \frac{h_{abs}(c_{eq}-c_o)}{c_s(T_{eq}-T_o)} \tag{23}$$

$$Le = \frac{\alpha}{D_s} \tag{24}$$

3.2. Compact equations for heat and mass transfer

For the sake of brevity, the details of the LTM implementation have been highlighted in Appendix B. Also, the procedure for generalizing the present analytical model for different absorber configurations has been explained in Appendix C. By finding the temperature and concentration distributions using Eqs. (B.25) and (B.26), see Appendix. B., the HMT rates for the absorption process in the falling film can be calculated as follows:

$$\dot{q}(\xi) = \frac{k_s(T_{eq}-T_o)}{\delta}\frac{\partial\theta}{\partial\eta}|_{inf}\left[\frac{w}{m^2}\right] \tag{25}$$

$$\dot{m}(\xi) = \frac{\rho_s D_s(c_{eq}-c_o)}{\delta}\frac{\partial\gamma}{\partial\eta}|_{inf}\left[\frac{kg}{m^2.s}\right] \tag{26}$$

where, k_s, ρ_s, and D_s are the solution thermal conductivity, density, and mass transfer coefficient, respectively. However, analogous to previous analytical solutions, this requires performing tedious calculations and may not be applicable for real-time system operation and optimization. Therefore, in this study, new compact relationships are proposed based on the above analytical solution using curve fitting techniques. The proposed solution is also extended to other geometries and new compact relationships are developed. Table 2 summarizes these proposed compact equations to calculate the HMT for absorption falling films over an inclined plate, vertical tube, horizontal tube, and coil type absorbers. The corresponding constants have been presented in Table 3.

Table 2
Compact equations to find the HMT for absorption falling films over inclined plate, vertical tube, horizontal tube, and coil type absorbers.

Parameter	Equation	
Local heat transfer, $\dot{q}_l$ [$\frac{w}{m^2}$]	$B_1.\frac{Le}{\Lambda}.(1-1.06\theta_w)(C_1e^{A_1x}+C_3e^{A_2x})$	(27)
Local absorption rate, $\dot{m}_l$ [$\frac{kg}{m^2s}$]	$B_2(1-1.06\theta_w)(C_1e^{A_1x}+C_3e^{A_2x})$	(28)
Total heat transfer, $\dot{q}_t$ [$\frac{w}{m}$]	$B_1.\frac{Le}{\Lambda}.(1-1.06\theta_w)[\frac{C_1}{A_1}(e^{A_1L_c}-1)+\frac{C_3}{A_2}(e^{A_2L_c}-1)]$	(29)
Total absorption rate, $\dot{m}_t$ [$\frac{kg}{ms}$]	$B_2(1-1.06\theta_w)[\frac{C_1}{A_1}(e^{A_1L_c}-1)+\frac{C_3}{A_2}(e^{A_2L_c}-1)]$	(30)
$\Lambda=\frac{h_{abs}(c_{eq}-c_o)}{c_s(T_{eq}-T_o)}$ $Le=\frac{\alpha}{D_s}$	$B_1=\frac{k_s(T_{eq}-T_0)}{A_3\delta}$ $B_2=\frac{\rho_s.D.(c_{eq}-c_0)}{A_3\delta}$	

4. Results and discussion

4.1. Model validation

In this section, the compact equations and available experimental data are compared to validate the proposed compact models. Table 4 lists the operating conditions and configuration of the available experimental data from the Refs. [37–40] used for the comparisons. The properties of the LiBr-water solution used for obtaining the results are listed in Table 5.

Fig. 3 shows the absorption rate versus vapor pressure calculated using the present model, Eq. (30), the analytical model of Meyer and Ziegler [30] (Eq. (51) in Ref. [30]), and the analytical model of Mortazavi and Moghaddam [32] (Eq. (42) in Ref. [32]) compared against the experimental data from Islam [37]. The average relative difference between the present analytical model compared to the experimental data of Islam [37] is 18.4%; while the Meyer and Ziegler [30] and Mortazavi and Moghaddam [32] models show the average relative differences of 31.9% and 28.8%, respectively. Therefore, it can be concluded that the present velocity profile used for obtaining the compact equation can enhance the accuracy.

Fig. 4 shows the absorption rate variation versus LiBr-water solution mass flow rate calculated using the present model, Eq. (30), compared to the experimental data collected by Yoon et al. [38] (coil type absorber) and Miller and Perez-Blanco [39] (vertical tube). The maximum and average relative differences of the present model compared to the both experimental data [38,39] are 16.9% and 8.1%., respectively.

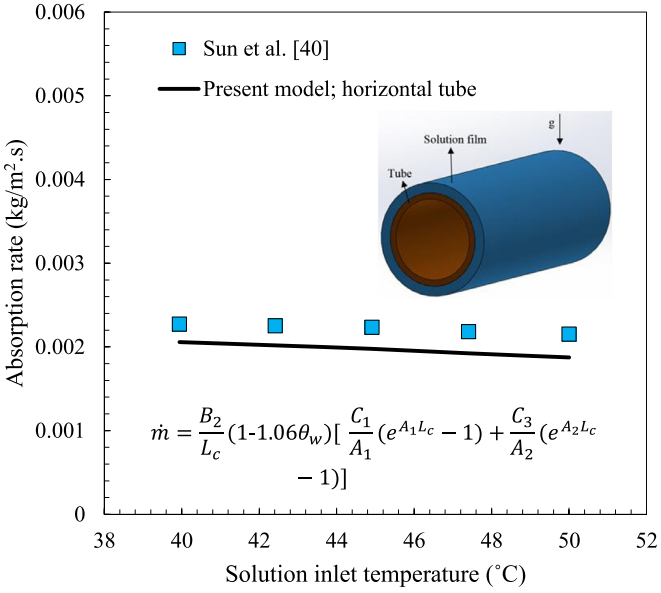

Fig. 5. Absorption rate variation versus solution inlet temperature calculated using the present model (Eq. (30)), compared against the experimental data from Sun et al. [40].

Fig. 5 demonstrates the absorption rate variation versus the solution inlet temperature calculated using the present model, Eq. (30), compared against experimental data from Sun et al. [40] (tube bundles absorber). The maximum and average relative

Table 3
Corresponding constants for the equations listed in Table 2.

Constant	Horizontal tube	Helical (coil)	Inclined plate	Vertical tube
	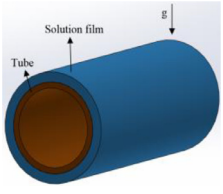	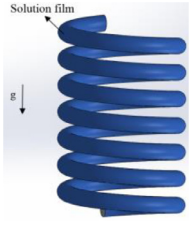	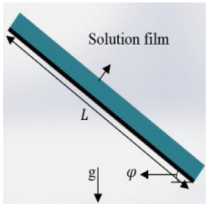	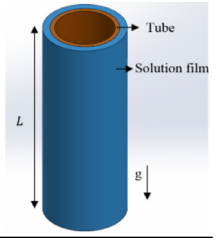
A_1	$1.33\frac{C_2}{\mathbb{C}}$	$1.33\frac{C_2}{\mathbb{C}}$	$\frac{C_2}{\mathbb{C}}\sin^{\frac{1}{3}}(\varphi)$	$\frac{C_2}{\mathbb{C}}$
A_2	$1.33\frac{C_4}{\mathbb{C}}$	$1.33\frac{C_4}{\mathbb{C}}$	$\frac{C_4}{\mathbb{C}}\sin^{\frac{1}{3}}(\varphi)$	$\frac{C_4}{\mathbb{C}}$
A_3	1.33	1.2	1	1
L_c	$\frac{N_{tube}\pi D_{tube}}{2}$	$\frac{N_{turn}\pi D_{tube}}{2}$	L	L
$C_1=\left(\frac{-21.12\ LEA^{0.9837}-1.158}{-7.805\ LEA-18.47}\right)(0.0005169\ Le+1)$				$10<Le<150$
$C_2=\left(\frac{-6.825\ LEA^{1.108}-22.06}{-9.639\ LEA-30.25}\right)(-4.09\ Le^{-0.9895}+1)-1.815\ LEA^{0.05511}+1.192$				$5<LEA=\frac{Le}{\Lambda}<100$
$C_3=\left(\frac{4.222\ LEA^{0.992}-3.43}{6.384\ LEA+56.21}\right)(0.6293\ Le^{0.5484}+1)-0.00386\ Le$				
$C_4=\left(\frac{-6.192\ LEA^{0.7131}-28.91}{-28.43\ LEA-26.73}\right)(10.11\ Le^{-0.6652}+1)-13.02\ Le^{-0.6467}$				
$C_1=\left(\frac{-27.31\ LEA^{0.8728}+45.21}{-1.938\ LEA-50.23}\right)(0.0008767\ Le+1)$				$150<Le<1000$
$C_2=\left(\frac{124.3\ LEA^{0.2306}+312.6}{1.865\ LEA^{0.1673}+236.6}\right)(-1.172\ Le^{-0.1688}+1)-1.001\ LEA^{0.1285}-0.0001122\ Le$				$5<LEA=\frac{Le}{\Lambda}<100$
$C_3=\left(\frac{-32.37\ LEA^{-0.06114}-23.04}{-116.8\ LEA^{-0.567}-83.16}\right)(2.333\ Le^{0.2041}+1)-0.1971\ Le^{0.3514}-0.0008664\ LEA$				
$C_4=\left(\frac{3.817\ LEA^{-0.188}-18.35}{-2.496\ LEA^{0.9209}-4.126}\right)(-0.971\ Le^{0.003804}+1)-2.446\ Le^{-0.8613}$				
$\mathbb{C}=\frac{3}{2}\left(\frac{3\nu\Gamma^4}{g\rho^4\alpha^3}\right)^{1/3}$				–

Table 4
Operating conditions and configuration of the data from Refs. [37–40].

Study	Configuration	L or $\pi N_{tube} D_{tube}$ (m)	Γ (kg/ms)	$P_v (kPa)$	T_o (^oC)	T_w (^oC)	$c_o (kg/kg)$
Islam [37]	Horizontal tube	0.71	0.044	1–3	40	32	0.40
Yoon et al. [38]	Helical (coil)	0.25	0.01–0.04	1	45	28–30	0.40
Miller and Perez-Blanco [39]	Vertical tube	1.4	0.1–0.2	1.3	52.4	46	0.38
Sun et al. [40]	Horizontal tube	0.45	0.0132	2.13	40–50	29	0.41

Table 5
Properties of LiBr-water solution [26,32].

Thermophysical property	Value
Dynamic viscosity (Pa.s)	0.005
Density (kg.m^{-3})	1500
Thermal conductivity (W.m^{-1}·K^{-1})	0.42
Specific heat capacity (kJ.kg^{-1} K^{-1})	2
Absorption heat (kJ.kg^{-1})	2500
Lewis number	100

Table 6
Base values and ranges used for the parametric study.

Parameter	Value	Range
Inlet temperature, T_o (^oC)	40	32–48 (± 20%)
Wall temperature, T_w (^oC)	30	24–36 (± 20%)
Inlet solution concentration, $1 - c_o(\frac{kg\ LiBr}{kg\ solution})$	0.6	0.56–0.64 (± 10%)
Absorber chamber pressure, p_v (Pa)	1100	872–1320 (± 20%)
Solution flow rate, Γ $(\frac{kg}{m.s})$	0.08	0.065–0.095 (± 20%)

differences between the present model and the experimental data [40] are 12.8% and 11.1%, respectively.

4.2. Parametric study

In this section, a parametric study has been conducted using the present analytical model (for falling film over a vertical plate with a length of 1 m) to investigate the effect of key parameters, including inlet temperature, wall temperature, inlet concentration, solution mass flow rate, and absorber chamber pressure on the absorption rate. Table 6 lists the base values and ranges of the above-mentioned parameters, which are selected arbitrarily for this parametric study. The vertical plate length and the operating conditions were selected based on the real applicable values, see Table 4. The LiBr-water solution properties listed in Table 5 are used for the parametric study.

Fig. 6 shows the absorption rate variation versus the solution inlet temperature, wall temperature, solution inlet concentration, vapor pressure, and solution mass flow rate for a vertical plate with a length of 1 m. The following can be observed:

(i) Solution inlet concentration is the most important parameter in absorption rate enhancement, while the solution mass flow rate is the least effective one.
(ii) As expected, lowering solution inlet temperature and wall temperature results in absorption rate enhancement since a higher temperature will lead to lower absorption rate; and
(iii) Increasing solution inlet concentration, vapor pressure, and solution mass flow rate leads to absorption rate enhancement.

4.3. Temperature and concentration profiles

This section provides an in-depth concept of the HMT phenomenon for the falling film absorption process. To obtain temperature and concentration profiles over a vertical plate, the following input parameters are used: Le= 100, $\mathbf{\Lambda}$= 10, and $\boldsymbol{\theta_w}$= −1. Fig. 7(a) shows non-dimensional temperature profiles versus "η" along the film flow direction, non-dimensional "x" or "ξ", obtained by the present analytical solution. The following from Fig. 7(a) can be observed:

(i) At the falling film's entrance region, two TBLs are formed: (i) a TBL, which is adjacent to the wall, due to temperature difference between the wall and film temperatures, and (ii) another TBL, which is in the vicinity of the vapor-solution interface, as a consequence of the temperature difference between fluid and the interface temperatures. Therefore, the flow between the two TBLs does not sense the heat transferred from the wall or the vapor-solution interface, and the flow temperature is equal to the inlet temperature. This phenomenon can be observed in Fig. 7(b) illustrating the non-dimensional temperature versus "η" at ξ= 0.001;
(ii) With increasing ξ, the two TBLs merge and the temperature profile becomes nearly linear; and
(iii) Downstream, the film temperature, from the wall to the vapor-solution interface, is virtually equal to the wall temperature since the film is thin (∼1 mm).

Fig. 7(c) shows the non-dimensional temperature along the film flow direction, non-dimensional "x" or "ξ", at different "η". The following from Fig. 7(c) can be observed:

(i) At the falling film's entrance region (low ξ), the temperature of the solution close to the vapor-solution interface (η= 0.8 and 1) increases due to the heat generation during absorption process.
(ii) At the falling film's entrance region (low ξ), the temperature of the solution close to the wall drops extremely due to sensing the TBL adjacent to the wall; and
(iii) Downstream, the temperature of the entire film reaches the wall temperature.

Fig. 8(a) shows non-dimensional concentration profiles "η" along the film flow direction, non-dimensional "x" or "ξ", obtained by the present analytical solution. From Fig. 8(a), the following can be concluded:

(i) At the entrance region, the CBL thickness is quite small. The CBL can be observed in Fig. 8(b); and
(ii) The absorption rate shows an almost linear relationship with the concentration difference at the vapor-solution interface, see Eq. (26). Downstream, the concentration gradient at the vapor-solution interface decreases. Therefore, the absorption rate decreases.

Fig. 8(c) shows non-dimensional concentration profiles along the film flow direction, non-dimensional "x" or "ξ", at different "η". The following from Fig. 8(c) can be observed:

(i) At the entrance region (low "ξ"), except for the solution in the vicinity of the vapor-solution interface, the solution concentration is constant since the solution does not sense the CBL; and

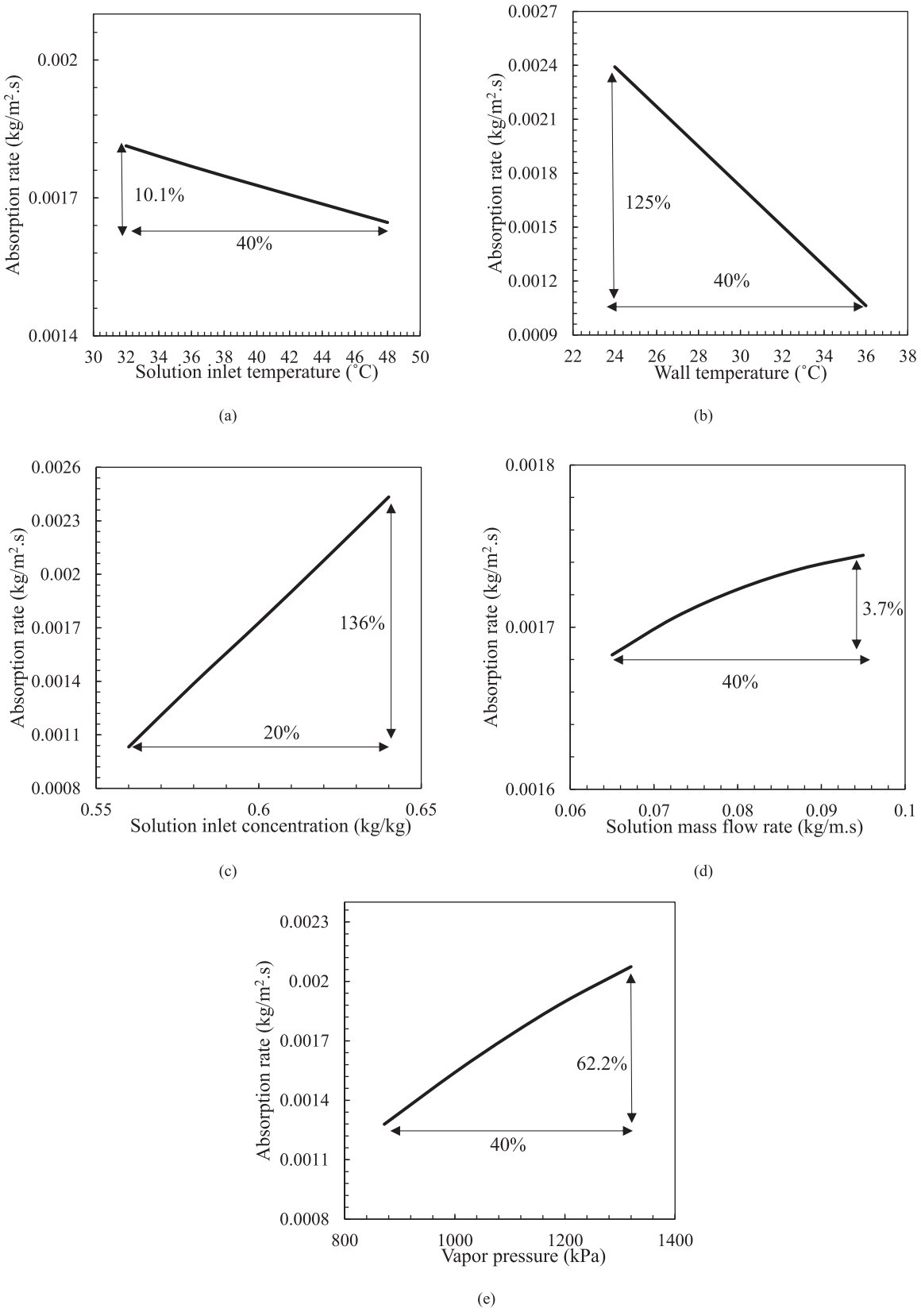

Fig. 6. A parametric study, investigating the effect of key input parameters on the present model absorption rate, Eq. (30), variation versus: (a) solution inlet temperature; (b) wall temperature; (c) solution inlet concentration; (d) vapor pressure; and (e) solution mass flow rate for a vertical plate with a length of 1 m.

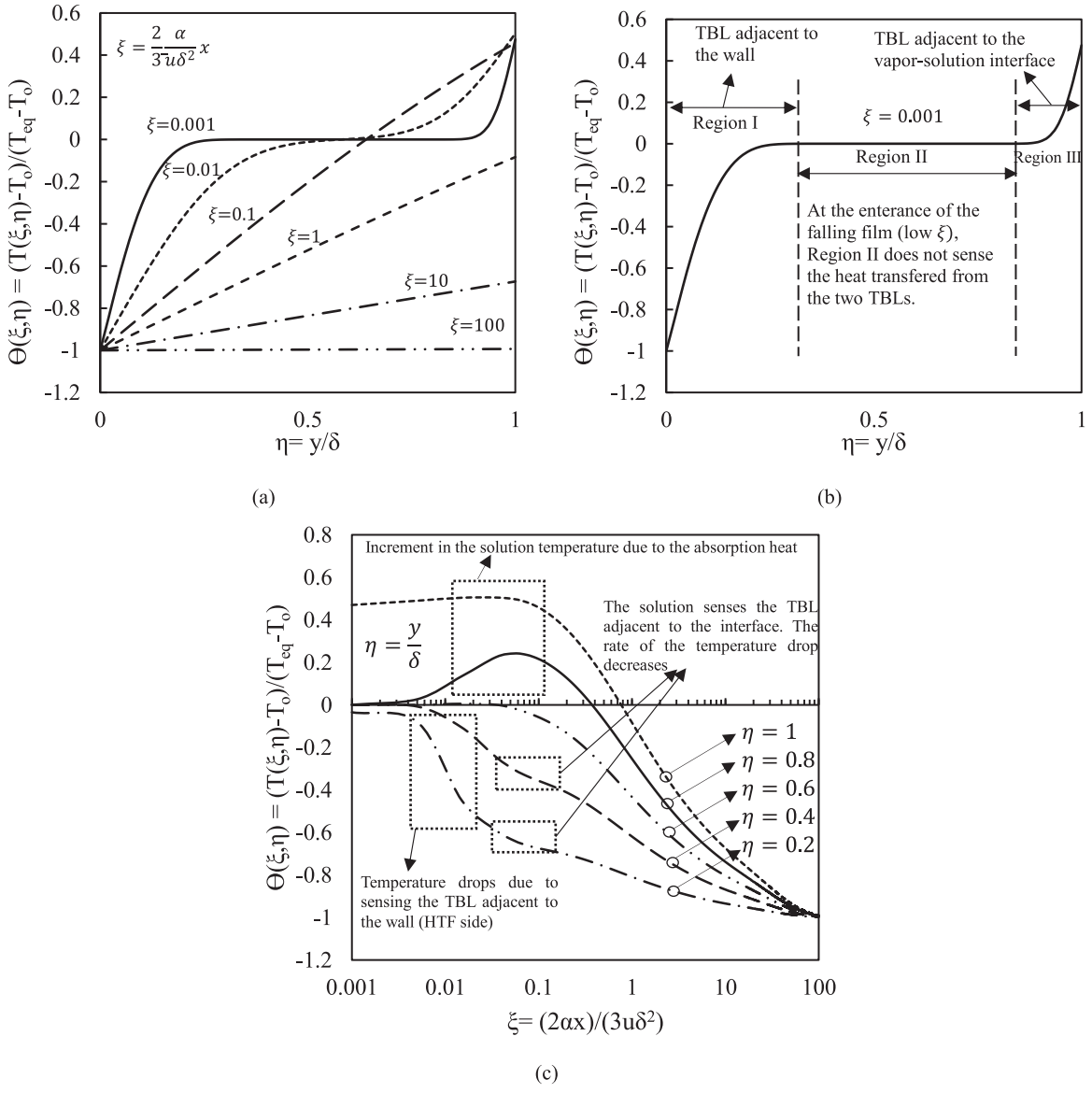

Fig. 7. (a) Non-dimensional temperature versus "η" at different non-dimensional "x" or "ξ"; (b) (a) non-dimensional temperature versus "η" at $\xi = 0.001$ which illustrates TBLs; and (c) non-dimensional temperature versus "ξ" at different "η", which are obtained by the present analytical solution at Le= 100, $\mathbf{\Lambda}$= 10, and $\boldsymbol{\theta}_{\mathbf{w}} = -1$.

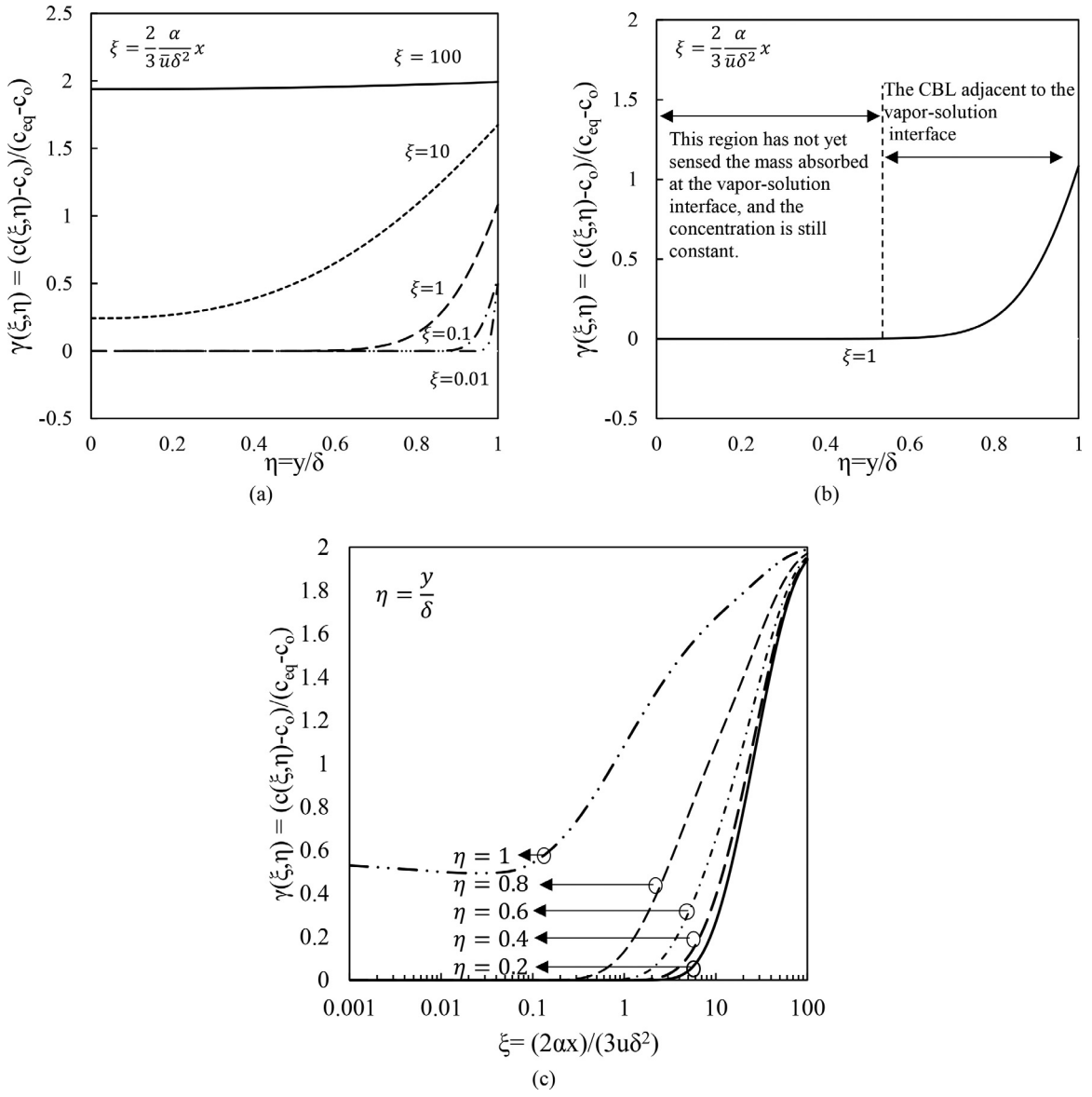

Fig. 8. (a) Non-dimensional concentration versus "η" at different non-dimensional "x" or "ξ"; (b) (a) non-dimensional concentration versus "η" at $\xi = 0.001$ which illustrates TBLs; and (c) non-dimensional concentration versus "ξ" at different "η", which are obtained by the present analytical solution at Le= 100, Λ=10, and $\theta_w = -1$.

(ii) Downstream, the concentration of the entire solution film reaches the vapor-solution interface concentration.

5. Conclusion

In this study, a new analytical solution was presented based on the Laplace transform method by proposing a new velocity profile. It was shown that the new velocity profile leads to more accurate results compared to the previous uniform or linear velocity profile. Moreover, for the first time, compact relationships based on the present model were proposed to calculate the HMT rate in falling film absorption. The present model was extended to include three common absorber configurations, including: (i) a vertical tube; (ii) a horizontal tube; and (iii) a helical absorber. The proposed compact equations were validated with experimental data available in the literature. Also, a parametric study was conducted showing that the solution inlet concentration was the most effective parameter in absorption rate enhancement, and solution mass flow rate had the least effect.

Declaration of Competing Interest

The authors declare that they have no known competing financial interests or personal relationships that could have appeared to influence the work reported in this paper.

CRediT authorship contribution statement

Mahyar Ashouri: Conceptualization, Software, Writing – original draft. **Majid Bahrami:** Conceptualization, Writing – review & editing, Supervision, Project administration, Funding acquisition.

Acknowledgments

This research is supported by funding from the Pacific Institute for Climate Solutions (PICS) Opportunity (Grant No. 36170-50280) and NSERC Advancing Climate Change Science in Canada (Grant No. 536076-18).

Appendices

Appendix. A. Equation for the phase equilibrium of an LiBr-water solution

The following experimental correlation [30] can be used to calculate the equilibrium temperature and concentration for an LiBr-water solution [30]:

$$\begin{aligned}-\frac{1}{T} = {} & a_1 + a_2(1-c) + a_3 \ln\left(\frac{1}{Pa}.p\right) + a_4(1-c)\ln\left(\frac{1}{Pa}.p\right) + a_5(1-c)^2 + a_6\ln^2\left(\frac{1}{Pa}.p\right) \\ & + a_7(1-c)^2\ln\left(\frac{1}{Pa}.p\right) + a_8(1-c)\ln^2\left(\frac{1}{Pa}.p\right) + a_9(1-c)^2\ln^2\left(\frac{1}{Pa}.p\right) \\ & + a_{10}(1-c)^3 + a_{11}\ln^3\left(\frac{1}{Pa}.p\right) + a_{12}(1-c)^3\ln\left(\frac{1}{Pa}.p\right) \\ & + a_{13}(1-c)^3\ln^2\left(\frac{1}{Pa}.p\right) + a_{14}(1-c)\ln^3\left(\frac{1}{Pa}.p\right) + a_{15}(1-c)^2\ln^3\left(\frac{1}{Pa}.p\right) \\ & + a_{16}(1-c)^3\ln^3\left(\frac{1}{Pa}.p\right) \end{aligned} \tag{A.1}$$

where, $\boldsymbol{T}$, $\boldsymbol{c}$, and $\boldsymbol{p}$, are temperature, LiBr concentration, and pressure, respectively. Also, $\boldsymbol{a}_{1\ to\ 16}$ are the corresponding constants, which are represented in Table A.1.

Table A.1
Constants for the phase equilibrium Eq. (2) [30].

Constant	Value
$\boldsymbol{a}_1$	-4.70858×10^{-3}
$\boldsymbol{a}_2$	-1.276757×10^{-3}
$\boldsymbol{a}_3$	1.45597×10^{-4}
$\boldsymbol{a}_4$	4.28261×10^{-4}
$\boldsymbol{a}_5$	9.48526×10^{-4}
$\boldsymbol{a}_6$	3.47501×10^{-6}
$\boldsymbol{a}_7$	-4.95401×10^{-4}
$\boldsymbol{a}_8$	-5.44472×10^{-5}
$\boldsymbol{a}_9$	1.10477×10^{-4}
$\boldsymbol{a}_{10}$	4.915398×10^{-3}
$\boldsymbol{a}_{11}$	-7.21234×10^{-8}
$\boldsymbol{a}_{12}$	-5.8121×10^{-4}
$\boldsymbol{a}_{13}$	-2.23738×10^{-5}
$\boldsymbol{a}_{14}$	2.39788×10^{-6}
$\boldsymbol{a}_{15}$	-6.64049×10^{-6}
$\boldsymbol{a}_{16}$	4.26683×10^{-6}

Appendix. B. Laplace transform solution

At first, boundary conditions Eqs. (19)–((22)) should be converted by taking the Laplace transform with respect to variable "$\boldsymbol{\xi}$"

$$\Theta(s,0) = \frac{\theta_w}{s} \tag{B.1}$$

$$\frac{\partial \mathrm{Y}(\boldsymbol{s},\eta=0)}{\partial\eta} = 0 \tag{B.2}$$

$$\Theta(s,\eta=1) + \mathrm{Y}(s,\eta=1) = \frac{1}{\boldsymbol{s}} \tag{B.3}$$

$$\frac{\partial\ \Theta(s,\eta=1)}{\partial\eta}|_{inf} = \frac{\Lambda}{Le}\frac{\partial\ \mathrm{Y}(s,\eta=1)}{\partial\eta}|_{inf} \tag{B.4}$$

Likewise, by taking the Laplace transform from Eqs. (12) and (13), they can be transformed into

$$s.\sqrt{\eta}\Theta(s,\eta) = \frac{\partial^2\Theta(s,\eta)}{\partial\eta^2} \tag{B.5}$$

$$s.Le.\sqrt{\eta}\mathrm{Y}(s,\eta) = \frac{\partial^2\mathrm{Y}(s,\eta)}{\partial\eta^2} \tag{B.6}$$

Replacing variable "$\boldsymbol{\eta}$" with $\boldsymbol{z} = \boldsymbol{s}^{0.4}\boldsymbol{\eta}$, Eqs. (B.5) and (B.6) are transformed into

$$\frac{d^2\Theta}{dz^2} - \sqrt{z}\Theta = 0 \tag{B.7}$$

$$\frac{d^2\mathrm{Y}}{dz^2} - Le\sqrt{z}\mathrm{Y} = 0 \tag{B.8}$$

The solution to Eqs. (B.7) and (B.8) can be obtained using the modified Bessel function of the first and second kinds

$$\Theta(s,\eta) = c_1\sqrt{s^{0.4}\eta}\ I_{\frac{2}{5}}\left(\frac{4}{5}\left(s^{0.4}\eta\right)^{\frac{5}{4}}\right) + c_2\sqrt{s^{0.4}\eta}\ K_{\frac{2}{5}}\left(\frac{4}{5}\left(s^{0.4}\eta\right)^{\frac{5}{4}}\right) \tag{B.9}$$

$$\mathrm{Y}(s,\eta) = c_3\sqrt{s^{0.4}\eta}\ I_{\frac{2}{5}}\left(\frac{4}{5}\sqrt{Le.s}(\eta)^{\frac{5}{4}}\right) + c_4\sqrt{s^{0.4}\eta}\ K_{\frac{2}{5}}\left(\frac{4}{5}\sqrt{Le.s}(\eta)^{\frac{5}{4}}\right) \tag{B.10}$$

where, $\boldsymbol{c}_1$, $\boldsymbol{c}_2$, $\boldsymbol{c}_3$, and $\boldsymbol{c}_4$ are constants, related to operating conditions and the properties of a working pair, which are as follows:

$$c_1 = \frac{s^{-1.2} - c_2k_2 - \frac{Le}{\Lambda}c_2\beta_2H}{k_1 + \frac{Le}{\Lambda}\beta_1H} \tag{B.11}$$

$$c_2 = \frac{m\theta_w}{s} \tag{B.12}$$

$$c_3 = nc_4 \tag{B.13}$$

$$c_4 = \frac{Le}{\Lambda}\frac{c_1\beta_1 + c_2\beta_2}{n\ \beta_3 + \beta_4} \tag{B.14}$$

$$H = \frac{n\ k_3 + k_4}{n\ \beta_3 + \beta_4} \tag{B.15}$$

$$\beta_1 = p.k_1 + \frac{q}{\sqrt{Le}}\left(k_5 + \frac{2}{5a}\ k_1\right) \tag{B.16}$$

$$\beta_2 = p.k_2 + \frac{q}{\sqrt{Le}}\left(k_6 + \frac{2}{5a}\ k_2\right) \tag{B.17}$$

$$\beta_3 = p.k_3 + q\left(k_7 + \frac{2}{5b}\ k_3\right) \tag{B.18}$$

$$\beta_4 = p.k_4 + q\left(k_8 + \frac{2}{5b}\ k_4\right) \tag{B.19}$$

$$k_1 = I_{\frac{2}{5}}(a),\ k_2 = K_{\frac{2}{5}}(a),\ k_3 = I_{\frac{2}{5}}(b),\ k_4 = K_{\frac{2}{5}}(b) \tag{B.20}$$

$$k_5 = I_{\frac{7}{5}}(a),\ k_6 = K_{\frac{7}{5}}(a),\ k_7 = I_{\frac{7}{5}}(b),\ k_8 = K_{\frac{7}{5}}(b) \tag{B.21}$$

$$p = 0.5\ s^{0.2},\ q = \sqrt{Le}\ s^{0.7} \tag{B.22}$$

$$a = \frac{4}{5}\sqrt{s},\ b = \frac{4}{5}\sqrt{Le.s} \tag{B.23}$$

$$m = 0.62497,\ n = 1.6516 \tag{B.24}$$

Finally, by taking the inverse Laplace transform from Eqs. (B.9) and (B.10) using the Stehfest method [20], the temperature and concentration profile can be obtained

$$\theta(\xi,\eta)=\frac{ln2}{\xi}\sum_{i=1}^{N}V_i\Theta\left(\frac{ln2}{\xi}i,\eta\right) \tag{B.25}$$

$$\gamma(\xi,\eta)=\frac{ln2}{\xi}\sum_{i=1}^{N}V_i Y\left(\frac{ln2}{\xi}i,\eta\right) \tag{B.26}$$

where, $\boldsymbol{V_i}$ is defined as follows:

$$V_i=(-1)^{\frac{N}{2}+j}\sum_{k=\left[\frac{j+1}{2}\right]}^{\min\left(j,\frac{N}{2}\right)}\frac{k^{\frac{N}{2}}(2k)!}{\left(\frac{N}{2}-k\right)!k!(k-1)!(j-k)!(2k-j)!} \tag{B.27}$$

Appendix. C. Solution generalization

To generalize the analytical solution for calculating the heat and mass transfer over an inclined plate to other geometries, the average film thickness should be calculated by integrating Eq. (4) from 0 to π. For instance, to calculate the heat and mass transfer over a horizontal tube with circular cross section, as shown in Fig. C. 1, the following average film thickness is obtained:

$$\delta_{ave}=\frac{1}{\pi}\int_0^{\pi}\left(\frac{3\Gamma\nu}{g\rho sin(\varphi)}\right)^{1/3}d\varphi=1.33\ \delta_{vertical\ \ plate} \tag{C.1}$$

The average film thickness is then used to calculate the average velocity and non-dimensional tangential distance ξ:

$$\overline{u}=\frac{\Gamma}{\rho_s\delta_{ave}} \tag{C.2}$$

$$\xi=\frac{2}{3}\frac{x}{\delta_{ave}^2}\frac{\alpha}{\overline{u}}=\frac{2}{3}\frac{x}{\delta_{ave}}\frac{\alpha\rho_s}{\Gamma} \tag{C.3}$$

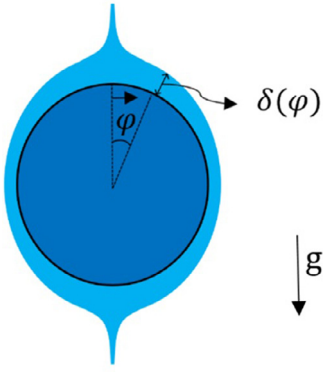

Fig. C. 1. Schematic diagram of the solution film over a horizontal tube.

References

[1] A. Salari, M. Ashouri, A. Hakkaki-Fard, On the performance of inclined rooftop solar chimney integrated with photovoltaic module and phase change material: a numerical study, Sol. Energy 211 (2020) 1159–1169.

[2] M. Ashouri, A. Hakkaki-Fard, Improving the performance of the finned absorber inclined rooftop solar chimney combined with composite PCM and PV module, Sol. Energy 228 (2021) 562–574, doi:10.1016/J.SOLENER.2021.09.088.

[3] National Research Council Government of Canada. Energy Use Data Handbook Tables. 15 December 2004. Available online: https://oee.nrcan.gc.ca/corporate/statistics/neud/dpa/menus/trends/handbook/tables.cfm.

[4] I.E.A.D. of S.E. PolicyTransition to Sustainable Buildings: Strategies and Opportunities to 2050, Organization for Economic, 2013.

[5] H. Bahrehmand, M. Bahrami, Optimized Sorber bed heat and mass exchangers for sorption cooling systems, Appl. Therm. Eng. 185 (2021) 116348, doi:10.1016/j.applthermaleng.2020.116348.

[6] T. Wen, L. Lu, Y. Luo, Review on the fundamentals and investigations of falling film dehumidification/absorption refrigeration based on CFD technology, Int. J. Heat Mass Transf. 171 (2021) 121042.

[7] J. Wang, H. Li, X. Li, H. Cong, X. Gao, An intensification of mass transfer process for gas-liquid counter-current flow in a novel microchannel with limited path for CO_2 capture, Process Saf. Environ. Prot. 149 (2021) 905–914.

[8] M. Amani, S. Foroushani, M. Sultan, M. Bahrami, Comprehensive review on dehumidification strategies for agricultural greenhouse applications, Appl. Therm. Eng. 181 (2020) 115979, doi:10.1016/j.applthermaleng.2020.115979.

[9] A.I. Adnan, M.Y. Ong, S. Nomanbhay, K.W. Chew, P.L. Show, Technologies for biogas upgrading to biomethane: a review, Bioengineering 6 (2019) 92, doi:10.3390/bioengineering6040092.

[10] N. Giannetti, A. Rocchetti, S. Yamaguchi, K. Saito, Heat and mass transfer coefficients of falling-film absorption on a partially wetted horizontal tube, Int. J. Therm. Sci. 126 (2018) 56–66, doi:10.1016/j.ijthermalsci.2017.12.020.

[11] J. Yoo, S. Han, Y. Nam, S. Jeong, Effect of shot-peening on the passive film formation and corrosion of carbon steel in LiBr aqueous solution, J. Mech. Sci. Technol. 34 (2020) 4037–4041.

[12] C. Zhai, W. Wu, Heat and mass transfer performance comparison of various absorbers/desorbers towards compact and efficient absorption heat pumps, Int. J. Refrig. 127 (2021) 203–220.

[13] N. Priyantha, P. Jayaweera, A. Sanjurjo, K. Lau, F. Lu, K. Krist, Corrosion-resistant metallic coatings for applications in highly aggressive environments, Surf. Coatings Technol. 163–164 (2003) 31–36. 10.1016/S0257-8972(02)00590-X.

[14] X. Liao, R. Radermacher, Absorption chiller crystallization control strategies for integrated cooling heating and power systems, Int. J. Refrig. 30 (2007) 904–911, doi:10.1016/j.ijrefrig.2006.10.009.

[15] M. Perier-Muzet, B. Stutz, Numerical study of the effectiveness of a vertical falling plate film absorber for an absorption chiller, Int. J. Refrig. 127 (2021) 221–229.

[16] A. Fasquelle, J. Pellé, S. Harmand, I.V. Shevchuk, Numerical study of convective heat transfer enhancement in a pipe rotating around a parallel axis, J. Heat Transf. 136 (5) (2014) 051901, doi:10.1115/1.4025642.

[17] I.V. Shevchuk, Modelling of Convective Heat and Mass Transfer in Rotating Flows, Springer, 2016.

[18] V.E. Nakoryakov, N.I. Grigoryeva, M.V. Bartashevich, Heat and mass transfer in the entrance region of the falling film: absorption, desorption, condensation and evaporation, Int. J. Heat Mass Transf. 54 (2011) 4485–4490, doi:10.1016/j.ijheatmasstransfer.2011.06.032.

[19] N. Giannetti, A. Rocchetti, S. Yamaguchi, K. Saito, Analytical solution of film mass-transfer on a partially wetted absorber tube, Int. J. Therm. Sci. 118 (2017) 176–186.

[20] Y. Wu, Simultaneous heat and mass transfer in laminar falling film on the outside of a circular tube, Int. J. Heat Mass Transf. 93 (2016) 1089–1099.

[21] V.E. Nakoryakov, N.I. Grigor'eva, Combined heat and mass transfer during absorption in drops and films, J. Eng. Phys. 32 (1977) 243–247, doi:10.1007/BF00865776.

[22] V.E. Nakoryakov, N.I. Grigor'Eva, Calculation of heat and mass transfer in non-isothermal absorption on the initial portion of a downflowing film, Theor. Found. Chem. Eng. 14 (1980) 483–488.

[23] V.E. Nakoryakov, N.I. Grigoreva, Heat and mass transfer in film absorption with varying liquid-phase volume, Theor. Found. Chem. Eng. 29 (3) (1995) 223–228.

[24] G. Grossman, Analysis of interdiffusion in film absorption, Int. J. Heat Mass Transf. 30 (1987) 205–208, doi:10.1016/0017-9310(87)90075-5.

[25] N. Brauner, D.M. Maron, H. Meyerson, Coupled heat condensation and mass absorption with comparable concentrations of absorbate and absorbent, Int. J. Heat Mass Transf. 32 (1989) 1897–1906.

[26] N. Giannetti, S. Yamaguchi, K. Saito, Simplified expressions of the transfer coefficients on a partially wet absorber tube, Int. J. Refrig. 105 (2019) 135–147, doi:10.1016/j.ijrefrig.2018.07.007.

[27] N.I. Grigor'eva, V.E. Nakoryakov, Exact solution of combined heat-and mass–transfer problem during film absorption, J. Eng. Phys. 33 (1977) 1349–1353.

[28] G. Grossman, Simultaneous heat and mass transfer in film absorption under laminar flow, Int. J. Heat Mass Transf. 26 (1983) 357–371, doi:10.1016/0017-9310(83)90040-6.

[29] V.E. Nakoryakov, N.I. Grigor'eva, L.V. Potaturkina, Analysis of exact solutions to heat-and mass-transfer problems for absorption with films or streams, Theor. Found. Chem. Eng. 31 (1997) 119–126.

[30] T. Meyer, F. Ziegler, Analytical solution for combined heat and mass transfer in laminar falling film absorption using first type boundary conditions at the interface, Int. J. Heat Mass Transf. 73 (2014) 141–151.

[31] T. Meyer, Analytical solution for combined heat and mass transfer in laminar falling film absorption with uniform film velocity-diabatic wall boundary, Int. J. Heat Mass Transf. 80 (2015) 802–811.

[32] M. Mortazavi, S. Moghaddam, Laplace transform solution of conjugate heat and mass transfer in falling film absorption process, Int. J. Refrig. 66 (2016) 93–104.

[33] A.T. Conlisk, Analytical solutions for the heat and mass transfer in a falling film absorber, Chem. Eng. Sci. 50 (1995) 651–660, doi:10.1016/0009-2509(94)00261-O.

[34] A.T. Conlisk, J. Mao, Nonisothermal absorption on a horizontal cylindrical tube-1. The film flow, Chem. Eng. Sci. 51 (1996) 1275–1285, doi:10.1016/0009-2509(95)00377-0.

[35] M.R. Conde, Properties of aqueous solutions of lithium and calcium chlorides: formulations for use in air conditioning equipment design, Int. J. Therm. Sci. 43 (2004) 367–382.

[36] M. Ashouri, M.M. Zarei, A. Moosavi, Investigation of the effects of geometrical parameters, eccentricity and perforated fins on natural convection heat transfer in a finned horizontal annulus using three dimensional lattice Boltzmann flux solver, Int. J. Numer. Methods Heat Fluid Flow (2021) In press, doi:10.1108/HFF-10-2020-0629.
[37] M.R. Islam, Absorption process of a falling film on a tubular absorber: an experimental and numerical study, Appl. Therm. Eng. 28 (2008) 1386–1394.
[38] J.I. Yoon, O.K. Kwon, P.K. Bansal, C.G. Moon, H.S. Lee, Heat and mass transfer characteristics of a small helical absorber, Appl. Therm. Eng. 26 (2006) 186–192.
[39] W.A. Miller, H. Perez-Blanco, Vertical-Tube Aqueous LiBr Falling Film Absorption Using Advanced Surfaces, Oak Ridge National Lab., TN (United States), 1993.
[40] J. Sun, L. Fu, S. Zhang, W. Hou, A mathematical model with experiments of single effect absorption heat pump using LiBr–H_2O, Appl. Therm. Eng. 30 (2010) 2753–2762.